

Non-Standard Models, Solar Neutrinos, and Large θ_{13}

R. Bonventre,¹ A. LaTorre,^{2,*} J.R. Klein,¹ G.D. Orebi Gann,^{2,3} S. Seibert,¹ and O. Wasalski^{2,†}

¹*Department of Physics and Astronomy, University of Pennsylvania, Philadelphia, PA 19104*

²*Department of Physics, University of California at Berkeley, Berkeley, CA 94720*

³*Nuclear Science Division, Lawrence Berkeley National Laboratory, Berkeley, CA 94720*

Solar neutrino experiments have yet to see directly the transition region between matter-enhanced and vacuum oscillations. The transition region is particularly sensitive to models of non-standard neutrino interactions and propagation. We examine several such non-standard models, which predict a lower-energy transition region and a flatter survival probability for the ^8B solar neutrinos than the standard large-mixing angle (LMA) model. We find that while some of the non-standard models provide a better fit to the solar neutrino data set, the large measured value of θ_{13} and the size of the experimental uncertainties lead to a low statistical significance for these fits. We have also examined whether simple changes to the solar density profile can lead to a flatter ^8B survival probability than the LMA prediction, but find that this is not the case for reasonable changes. We conclude that the data in this critical region is still too poor to determine whether any of these models, or LMA, is the best description of the data.

I. INTRODUCTION

With the recent precision measurements of θ_{13} [1, 2], the model of neutrino mixing is nearly complete. Of the seven new parameters added to the standard model to describe neutrino flavor transformation, only two remain unmeasured: the sign of the mass difference between the first and third mass eigenstates, and the value of the CP-violating phase δ . For a large fraction of neutrino transformation phenomenology, however, the current knowledge of the parameters is expected to be good enough to describe neutrino measurements very accurately. Much of the trust in the model comes from the fact that it neatly mirrors quark mixing, which has been subject to intense scrutiny for over four decades. Yet the model of neutrino mixing is still just that—a model—and until we test that model with the kind of precision with which we have explored the rest of particle physics, we do not know whether it is in fact a complete description of neutrinos.

Construction of a broad precision measurement program with neutrino oscillations suffers not only because of the difficulty in detecting neutrinos, but also because the model makes few predictions other than oscillations themselves. In vacuum, experiments can measure oscillation behavior very precisely, but any deviation seen between predicted transformation probability and observation must first be interpreted as a change to the mixing parameters, rather than new physics. A search for new physics thus relies primarily on looking for deviations from the L/E behavior that mass-difference-driven oscillations must have. Such searches can be sensitive to interesting new physics scenarios such as transformation to sterile neutrinos [3–5], or neutrino decay [6, 7].

The situation is dramatically different once neutrino passage through matter is considered. The weakness of neutrino interactions allows coherent processes - including those from new interactions or more exotic physics - to affect flavor transformation in a measurable way. Indeed, even in Wolfenstein's [8] seminal paper, he considers primarily the effects of flavor-changing neutral currents (FCNC) as a driver of neutrino flavor transformation in matter. Mikheyev and Smirnov [9] subsequently demonstrated that 'standard' oscillations in matter of varying density—such as that of the Sun—can lead to resonant flavor conversion. This implied that even tiny effects may be observable. MSW flavor transformation is an explicit prediction of the Standard Model and the model of neutrino oscillations. It states that given measured mixing parameters, which can be provided independently from solar neutrino measurements, and density profiles of the Sun and the Earth, the phenomenology of the MSW effect is exactly specified. Yet any interaction with matter that distinguishes neutrino states, even interactions weaker than the weak interaction itself, can spoil the agreement with MSW predictions. That precision measurements using solar neutrinos are possible has been demonstrated very clearly by the observed hints of non-zero θ_{13} that came out of comparing solar neutrino measurements with those of the KamLAND reactor experiment [10]. The precision of this comparison rivaled that of the measurements by the dedicated Double CHOOZ [11] experiment.

While many future experiments [12–14] are planned to terrestrially observe matter-enhanced oscillations, and thus look for non-standard effects, to date the only large observed matter enhancement is for solar neutrinos. In Fig. 1 we show the predictions of the survival probability for solar neutrinos, spanning the energy regime from the lowest-energy pp neutrinos to the highest-energy hep neutrinos. We show both a curve using just the mixing parameters as measured by KamLAND [15] and one with all solar data included, using the best-fit large-mixing angle (LMA) parameters. As has been pointed out by

* Present address: Department of Physics, University of Chicago, Chicago, IL 60637

† Present address: Department of Physics and Astronomy, University of British Columbia, Vancouver, BC V6T 1Z1, Canada

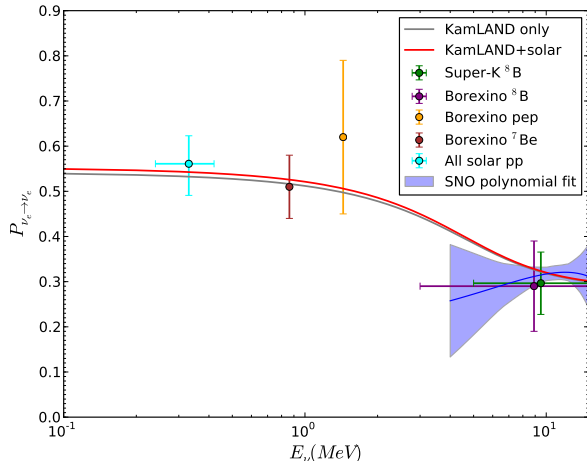


FIG. 1. (Color online) MSW prediction for $P_{\nu_e \rightarrow \nu_e}$ for the three-flavor KamLAND best fit parameters and the combined solar best fit parameters. Note that the *pep* uncertainties are not Gaussian and the value is only $\sim 2\sigma$ from zero. Data points for Borexino and S-K ^8B represent the survival probability averaged over the measured energy range.

many authors [16, 17], the predicted survival probability has three regimes. At high energies the effects of matter are pronounced, and thus the suppression of ν_e s exceeds the average value of $1 - 1/2 \sin^2 2\theta$ expected for just vacuum oscillations. At low energies vacuum effects are dominant, thus the survival probability matches the vacuum value. Between about 1 MeV and 4 MeV there is a transition region between the low- and high-energy regimes, where the survival probability decreases from the vacuum average to the matter-dominated value. It is in this transition region where non-standard effects would be most pronounced, as they interfere with the expectations from standard MSW transformation. As Nature would have it, probing this region is particularly difficult. Water Cherenkov experiments have poor energy resolution and hence difficulty getting below thresholds of 4 MeV, whereas scintillation experiments are typically either small or restricted to observing neutrinos through the elastic scattering of electrons, whose differential cross section is maximally broad.

Many authors [18–26] have put forth non-standard models and performed fits to the solar neutrino data set. Prior to the recent θ_{13} measurements, Palazzo [21] showed that non-standard interaction models provide a somewhat better fit to the solar neutrino data than does the standard MSW flavor transformation. The reason non-standard effects are preferred is the frustratingly persistent flatness of the high-energy solar ν_e survival probability, as measured by experiments observing ^8B neutrinos. In Figs. 2 and 3, we show the ^8B measurements from the Sudbury Neutrino Observatory (SNO), Borexino, and the Super-Kamiokande (S-K) experiments, with the expectation from large-mixing angle MSW effect su-

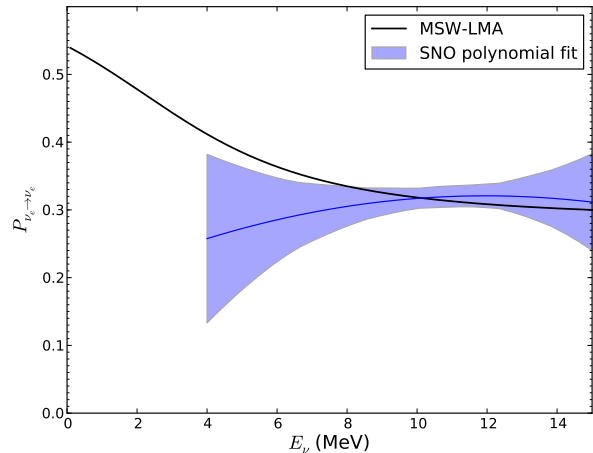


FIG. 2. (Color online) KamLAND’s combined best fit MSW-LMA prediction versus SNO extracted ^8B survival probability. The band represents the RMS spread at any given energy, i.e., not including energy correlations.

perimposed. We see that while the data is consistent with MSW, no experiment sees clear evidence of the expected rise due to the matter / vacuum transition region. The three experiments appear to differ in their comparison to the model: SNO fits the prediction best at high energies rather than low, while S-K is the reverse. In other words, SNO’s data appears to be flatter than predicted by MSW due to the fact that at low energies the survival probability fit is lower than the MSW curve, while S-K’s data appears to be flatter because the high energy event rate is higher than predicted by MSW, but in all cases the end result is that the data appears flatter than expected. The Borexino experiment’s uncertainties are clearly too large to make a meaningful comparison with their data alone.

In this paper we perform fits to the global solar neutrino data sets, including constraints on θ_{13} and the most recent measurements by the SNO collaboration. Section II describes each experiment we consider, how we simulate its results, and how we handle its statistical and systematic uncertainties. Section III describes our fitting procedure and our parameterization of the survival probability for each model we consider, and the results of the fit for each model are given in Section IV.

II. DATA SETS AND APPROACH

Our solar neutrino data sets include the weighted average of the results of the gallium experiments (SAGE, GALLEX, and GNO) given in Ref. [27], and separately the results of the Chlorine experiment [28]. These experiments provide integral measurements of several solar neutrino fluxes. For the ‘realtime’ experiments, which measure exclusive fluxes, we include the most recent SNO

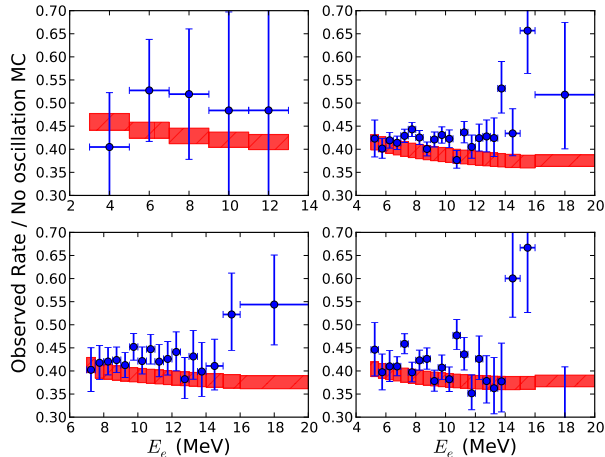


FIG. 3. (Color online) Top left: Borexino, top right: S-K I, bottom left: S-K II, bottom right: S-K III. Event rates binned in measured electron energy with each bin scaled by Monte Carlo predictions assuming GS98SF2 fluxes, versus the same ratio for the expected rates assuming KamLAND’s combined best fit LMA parameters and SNO’s NC ^8B flux prediction. Error bars on the data points represent statistical and energy uncorrelated systematic uncertainties combined in quadrature. Detector response parameters have been fixed at their reported value; the width of the band does not include the effect of correlated systematic uncertainties. The best fit oscillation prediction band width represents the uncertainty on the ^8B flux. Note that we have suppressed the zero for these figures to better illustrate the comparison between data and model.

results [29] for ^8B , the measurements of S-K I [30], S-K II [31], and S-K III [32] (which are also ^8B), and the measurements of Borexino for ^7Be [33], ^8B [34], and pep [35].

We follow the standard approach taken by other authors, except for the handling of the SNO results, for which explicit energy-dependent survival probabilities are provided. For all data sets other than SNO we predict the expected number of events either in a given energy bin or as an integral flux. To achieve this we convolve the neutrino energy spectrum with its interaction cross section on a given target, and the outgoing electron energy with the detector’s response. For a given oscillation hypothesis, we include in this integral the energy dependence of the survival probability. Because of the dependence on the production region within the Sun we calculate the survival probabilities separately for each solar neutrino source. The Super-Kamiokande collaboration has provided bin-by-bin “no-oscillation” spectra that include their full Monte Carlo detector model. Therefore for a given oscillation hypothesis we scale their numbers by the ratio of oscillation to no-oscillation calculated using the analytic Gaussian response they have provided.

Our survival probability calculation is an analytical approximation to a full three-flavor numerical integration of

the wave equation. We assume in all cases that $\Delta m_{31}^2/E$ is much larger than $\Delta m_{21}^2/E$ or any matter potential so the third flavor decouples and propagates independently of the other two. In addition, we assume adiabatic propagation in the Sun corrected by a two-flavor jump probability calculated at the resonance of maximal adiabaticity violation [36] (the results agree well with numerical calculations). We integrate over production location in the Sun for high metallicity model GS98SF2 [37] and low metallicity model AGSS09SF2 [38], using neutrino production and solar density distributions from each [39]. For the day-night effect we use the procedure described in Ref. [40], modeling the Earth as two spherical shells of constant density. We use a parameterized average annual solar exposure as described in Ref. [41]. Although we float the mixing parameters in our fits to data, we constrain them by known terrestrial measurements. For the dominant θ_{12} and Δm_{21}^2 parameters we use constraints from KamLAND [15], and constrain θ_{13} by the results of the Daya Bay [2] and RENO [1] collaborations.

Interaction cross sections for the Chlorine experiment are taken from Bahcall [42], including the estimated theoretical uncertainties. For the Gallium experiments, we assume zero strength for capture to the first two excited states of ^{71}Ge , as given in Appendix C of Ref. [27] of the SAGE collaboration. The remaining cross section has uncertainties that are highly asymmetric for certain energies. We follow Bahcall’s suggestion [43] and take a conservative approach that treats uncertainties for energies above 2 MeV and uncertainties below 2 MeV as being correlated with each group but not with each other. To handle the asymmetric nature of the uncertainties, we use a bifurcated Gaussian. For the elastic scattering cross section of electrons, which applies to Borexino and Super-Kamiokande, we use the cross section that includes radiative and electroweak corrections as given by Bahcall [44].

We consider all experimental uncertainties to be independent, with the exception of the three S-K measurements for which we treat the normalization uncertainties as being correlated across the three data sets. We have marginalized over systematic uncertainties for each experiment.

For Chlorine, Gallium, and Borexino, we check our reproduction of their data by comparing their no-oscillation flux predictions to our calculations. Borexino only gives a prediction for their integral measurement, but as mentioned earlier S-K provides binned no-oscillation predictions, allowing us to check our calculations more carefully. The binned predictions differ from our calculations by around a few percent per bin, which we assume to be due to unreported differences between the Gaussian detector response given in Ref. [32] and their full detector Monte Carlo. Once we scale our binned data by these differences, our integral flux predictions match within one percent.

For the results of the SNO collaboration, we can conveniently use the ν_e survival probability directly. To test

a given oscillation hypothesis against the SNO survival probability, we use the prescription described in Refs. [10] and [29]. The survival probability is projected onto the detected ^8B spectrum, and the quadratic form used by the SNO collaboration is extracted. In this way, the comparison comes down to a test of just six parameters: three for the day survival probability,

$$P_{ee}^{day}(E_\nu = c_0 + c_1(E_\nu[\text{MeV}] - 10) + c_2(E_\nu[\text{MeV}] - 10)^2, \quad (1)$$

two for the day-night asymmetry,

$$A_{ee}(E_\nu = a_0 + a_1(E_\nu[\text{MeV}] - 10), \quad (2)$$

and one for the ^8B flux scale.

III. FIT

Our interest is in reasonably generic non-standard models, especially those with the ability to flatten the ^8B survival probability. For this analysis we have chosen three types of models: non standard contributions to forward scattering as described in [18], mass varying neutrinos [22], and long-range leptonic forces [26].

We used these models to calculate survival probabilities, including the dominant standard MSW-LMA oscillation. We perform a maximum likelihood fit to the data, floating the standard mixing parameters ($\theta_{12}, \Delta m_{21}^2, \theta_{13}$) and various non-standard parameters for each model as well as the flux scaling for each neutrino production reaction and a systematic parameter for the shape of the ^8B spectrum [42]. Where we reference χ^2 in this paper we mean $-2 \log \mathcal{L}$. We constrain the values of the known mixing parameters to the values measured by the KamLAND collaboration [15] for the (1,2) sector, and the measurements of KamLAND, Daya Bay, and RENO for θ_{13} . The flux for each neutrino production reaction is constrained by the standard solar model values and uncertainties, although for ^8B the main constraint instead comes from SNO's NC measurement.

A. Non-Standard Forward Scattering

As suggested by Friedland in [18], one can generically parameterize these non-standard contributions with an effective low-energy four-fermion operator

$$\mathcal{L} = -2\sqrt{2}G_F(\bar{\nu}_\alpha\gamma_\rho\nu_\beta)(\epsilon_{\alpha\beta}^{f\tilde{f}P}\tilde{f}_P\gamma^\rho\tilde{f}_P) + h.c., \quad (3)$$

where $P=L,R$, and $\epsilon_{\alpha\beta}^{f\tilde{f}P}$ denotes the strength of the non-standard interaction between neutrinos of flavors α and β and the P handed components of fermions f and \tilde{f} . Only vector components where $f = \tilde{f}$ of the non-standard interaction can affect the neutrino propagation, so we let $\epsilon_{\alpha\beta}^f \equiv \epsilon_{\alpha\beta}^{ffL} + \epsilon_{\alpha\beta}^{ffR}$. One can define

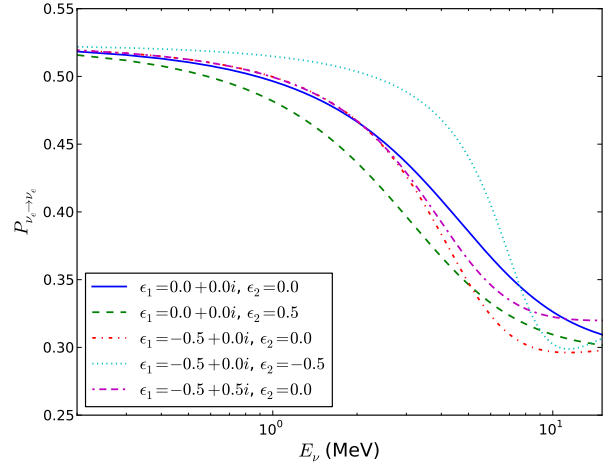


FIG. 4. (Color online) Survival probabilities for a range of the NSI parameters ϵ_1, ϵ_2

$\epsilon_{\alpha\beta} = \sum_{f=u,d,e} \epsilon_{\alpha\beta}^f n_f / n_e$. Then the matter part of the generic three flavor NSI oscillation Hamiltonian can be written as

$$\mathcal{H} = \sqrt{2}G_F n_e \begin{pmatrix} 1 + \epsilon_{ee} & \epsilon_{e\mu}^* & \epsilon_{e\tau}^* \\ \epsilon_{e\mu} & \epsilon_{\mu\mu} & \epsilon_{\mu\tau}^* \\ \epsilon_{e\tau} & \epsilon_{\mu\tau} & \epsilon_{\tau\tau} \end{pmatrix}. \quad (4)$$

As in our standard survival probability calculation, we assume the third flavor decouples and that the non-standard contribution to the potential is much smaller than $\Delta m_{31}^2/E$. Then the effective two flavor Hamiltonian is

$$\mathbf{H}^{2\nu} = \frac{\Delta m_{21}^2}{4E} \begin{pmatrix} -\cos 2\theta_{12} & \sin 2\theta_{12} \\ \cos 2\theta_{12} & \sin 2\theta_{12} \end{pmatrix} + \sqrt{2}G_F n_e \begin{pmatrix} \cos \theta_{13} & \epsilon_1^* \\ \epsilon_1 & \epsilon_2 \end{pmatrix} \quad (5)$$

where

$$\begin{aligned} \epsilon_1 &= c_{13}(\epsilon_{e\mu}c_{23} - \epsilon_{e\tau}s_{23}) \\ &\quad - s_{13}[\epsilon_{\mu\tau}s_{23}^2 - \epsilon_{\mu\tau}^*c_{23}^2 + (\epsilon_{\mu\mu} - \epsilon_{\tau\tau})c_{23}s_{23}], \\ \epsilon_2 &= \epsilon_{\mu\mu}c_{23}^2 - (\epsilon_{\mu\tau} + \epsilon_{\mu\tau}^*)s_{23}c_{23} + \epsilon_{\tau\tau}s_{23}^2 \\ &\quad + c_{13}^2\epsilon_{ee} + s_{13}[(e^{-i\delta}\epsilon_{e\mu} + e^{i\delta}\epsilon_{e\mu}^*)s_{23}c_{13} \\ &\quad + (e^{-i\delta}\epsilon_{e\tau} + e^{i\delta}\epsilon_{e\tau}^*)c_{13}c_{23}] \\ &\quad - s_{13}^2[\epsilon_{\mu\mu}s_{23}^2 + (\epsilon_{\mu\tau} + \epsilon_{\mu\tau}^*)s_{23}c_{23} + \epsilon_{\tau\tau}c_{23}^2]. \end{aligned} \quad (6)$$

We follow the example of Ref. [18] to calculate a modified mixing angle in matter as well as a jump probability to get a predicted survival probability.

This model adds up to three new parameters to the survival probability: $Re[\epsilon_1], Im[\epsilon_1], \epsilon_2$. Fig. 4 shows the effect of each one on the shape of the survival probability.

Current constraints on the strength of these vertices come from accelerator experiments like NuTeV and

CHARM, atmospheric neutrino and charged lepton experiments like LEP, and by limits on the charged lepton operators. The parameters $\epsilon_{e\mu}, \epsilon_{\mu\mu}$ are well constrained ($\lesssim 10^{-2} - 10^{-3}$), and analysis of atmospheric neutrino data has shown $\epsilon_{\mu\tau} \lesssim 10^{-2}$ [25]. However there remain vertices that can still be quite large, for example, $|\epsilon_{e\tau,ee}^f| \lesssim 0.5$, or $|\epsilon_{tt}^{dR}| < 6$.

By letting all the muon vertices go to zero, we get

$$\epsilon_1 = -c_{13}s_{23}\epsilon_{e\tau} + s_{13}c_{23}s_{23}\epsilon_{\tau\tau}, \quad (8)$$

$$\begin{aligned} \epsilon_2 = & s_{23}^2\epsilon_{\tau\tau} + c_{13}^2\epsilon_{ee} + s_{13}c_{13}c_{23}(e^{-i\delta}\epsilon_{e\tau} + e^{i\delta}\epsilon_{e\tau}^*) \\ & - s_{13}^2c_{23}^2\epsilon_{\tau\tau}. \end{aligned} \quad (9)$$

The effect of these non-standard parameters on the survival probability as a function of energy is shown in Fig. 4.

B. Mass Varying Neutrinos

1. Neutrino Density Effects

In Ref. [22] it was proposed that neutrinos are coupled to dark energy in a way that their energy densities track each other. This model was made to resolve the coincidence of the energy density of dark energy and matter being similar today even though their ratio scales as $\sim 1/(\text{scale factor})^3$. In general this implies so-called ‘Mass Varying Neutrinos’ (MaVaNs), where the neutrino mass becomes a function of the neutrino density. If the neutrino couples to a scalar field, then following Ref. [23] at low energy one can write an effective Lagrangian in a model independent way

$$\begin{aligned} \mathbf{L}(m_i) = & \sum_i [m_i \bar{\nu}_i^c \nu_i + m_i n_i^{C\nu B} \\ & + \int \frac{d^3k}{(2\pi)^3} \sqrt{k^2 + m_i^2} f_i(k) + V_0(m_i)]. \end{aligned} \quad (10)$$

Here $n_i^{C\nu B} = 112 \text{ cm}^{-3}$ is the number density of non-relativistic relic neutrinos of each type and $f_i(k)$ is the occupation number for momentum k of non-relic neutrinos in our medium (in this case a function of the neutrino production profile in the Sun). Then one can parameterize the scalar potential $V_0(m_i) \propto f(m_i/\mu)$ where μ is some arbitrary mass scale. The observed equation of state for dark energy implies that the potential must be flat, while minimizing the total potential implies it must decrease with increasing neutrino mass. Various forms for the scalar potential have been suggested, for example, $\log(\mu/m_i)$ or $(m_i/\mu)^{-\alpha}$. For either of these forms, minimizing the effective potential implies that

$$m_i(r) \approx m_{i,0} - |U_{e,i}|^2 A(r) m_{i,0}^2, \quad (11)$$

where $m_{i,0}$ is the vacuum mass of ν_i and

$$A(r) = \frac{1}{n^{C\nu B}} \int \frac{d^3k}{(2\pi)^3} \frac{1}{\sqrt{k^2 + m_i^2}} f_e(k, r). \quad (12)$$

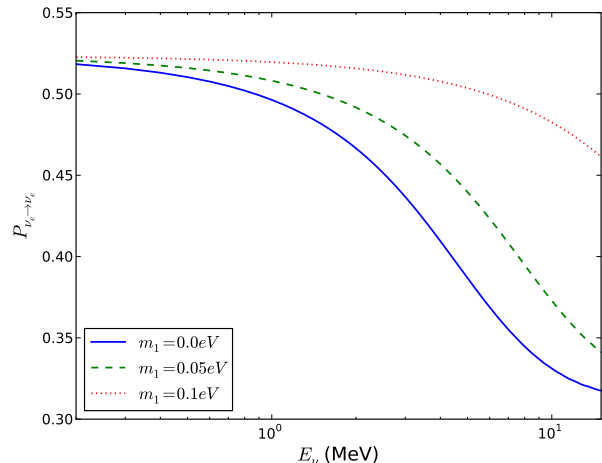


FIG. 5. (Color online) Survival probabilities for the neutrino density dependent MaVaN model at several values of $m_{1,0}$

Here we have used the fact that $f_i(k, r) = |U_{e,i}|^2 f_e(k, r)$ [23].

Then before MSW matter effects, we have

$$\begin{aligned} \Delta m_{21,eff}^2(r) = & m_2^2(r) - m_1^2(r) \\ \approx & \Delta m_{21,0}^2 [1 - 3s_{12}^2 c_{13}^2 A(r) m_{1,0}] \\ & + 2c_{13}^2 A(r) [c_{12}^2 - s_{12}^2] m_{1,0}^3, \end{aligned} \quad (13)$$

and we can solve for the survival probability by substituting this effective mass squared difference into the survival probability calculations for normal MSW oscillations. Then given a particular distribution of neutrinos, our effective mass squared difference becomes a function of the vacuum neutrino mass $m_{1,0}$. The survival probability for various values of the vacuum mass is shown in Fig. 5.

A previous two-flavor oscillation analysis of solar data and KamLAND found a 3σ upper limit of $m_{1,0} < 0.009 \text{ eV}$, with no improvement in the fit to the data over MSW-LMA [23].

2. Fermion Density Effects

In addition to the effect described above, it is possible for this scalar field to couple to visible matter. Ref. [24] parameterizes this model by adding a light scalar field ϕ of mass m_ϕ , which is weakly coupled to neutrinos and fermions;

$$\begin{aligned}
\mathbf{L} = & \sum_i \bar{\nu}_i (i\partial - m_{i,0}) \nu_i + \sum_f \bar{f} (i\partial - m_{f,0}) f \\
& + \frac{1}{2} \phi (\partial^2 - m_\phi^2) \phi + \sum_{ij} \lambda^{ij} \bar{\nu}_i \nu_j \phi \\
& + \sum_f \lambda^f \bar{f} f \phi. \tag{14}
\end{aligned}$$

Then the elements of the mass matrix become

$$\begin{aligned}
m_{ij}(r) &= m_{i,0} \delta_{ij} - M_{ij}(r), \\
M_{ij}(r) &= \frac{\lambda^{ij}}{m_\phi^2} \left(\sum_f \lambda^f n_f(r) \right. \\
& \left. + \sum_i \lambda^{ii} \int \frac{d^3k}{(2\pi)^3} \frac{M_{ii}}{\sqrt{k^2 + M_{ii}^2}} f_i(k, r) \right). \tag{15}
\end{aligned}$$

We will only consider the added effect of the coupling to fermionic matter by letting $m_{1,0} \sim 0$, such that

$$M_{ij}(r) = \frac{\lambda^{ij}}{m_\phi^2} \sum_f \lambda^f n_f(r). \tag{16}$$

Assuming that effect of this coupling is small compared to $m_{3,0}$, we can decouple the third neutrino state. Then diagonalizing the 1-2 sector for the mass eigenstates in matter gives

$$\cos 2\theta_{12}^m(r_0) = \frac{2\Delta m_{21}^2(r) \cos 2\theta_{12} - A(r)}{\Delta m_m^2} \tag{17}$$

where

$$\begin{aligned}
\Delta m_m^2 &= ((\Delta m_{21}^2(r))^2 + 4M_3^4(r) \\
& - 2A(r)\Delta m_{21}^2(r) \cos 2\theta_{12} + A^2)^{\frac{1}{2}}, \tag{18}
\end{aligned}$$

$$\Delta m_{21}^2(r) = (m_{2,0} - M_2(r))^2 - (m_{1,0} - M_1(r))^2, \tag{19}$$

and $M_{1,2,3}$ are linear combinations of the M_{ij} s, and can be parameterized as

$$M_i(r) = \alpha_i \rho(r) \tag{20}$$

for matter density $\rho(r)$. Then we can substitute the mixing angle in matter from Eq. 17 into our standard oscillation equations to get a survival probability as a function of our parameters α_i .

For the KamLAND constraint, we replace θ_{12} with θ_{12}^m and Δm_{21}^2 with Δm_m^2 as defined above except with $A \rightarrow -A$ and $\rho \sim 3\text{gr/cm}^3$ for the density of the Earth's crust. The survival probability for various values of the parameters α_i is shown in Fig. 6.

Current limits for the effective Yukawa coupling of any scalar with $m_\phi \gtrsim 10^{-11}\text{eV}$ to nucleons from tests of the inverse square law are $|\lambda^N| \lesssim 10^{-21}$ [22]. A previous two-flavor oscillation analysis of solar data plus KamLAND

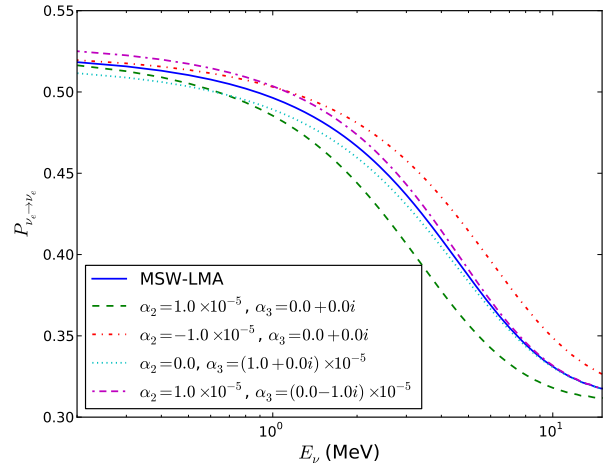


FIG. 6. (Color online) Survival probabilities for the fermion density dependent MaVaN model at several values of α_2, α_3

[24] found 90% confidence level bounds of

$$-2.2 \times 10^{-5} \leq \alpha_2/\text{eV} \leq 1.4 \times 10^{-4}, \tag{21}$$

$$|\alpha_3|/\text{eV} \leq 2.3 \times 10^{-5} \text{ for } \alpha_3^2 > 0, \tag{22}$$

$$|\alpha_3|/\text{eV} \leq 3.4 \times 10^{-5} \text{ for } \alpha_3^2 < 0. \tag{23}$$

C. Long-Range Leptonic Forces

We consider another group of generic non-standard interactions characterized by a new long-range force coupling to lepton flavor number. Since lepton flavor number is not conserved, such a force is likely to have a finite range. In general if the range is long enough, we follow Ref. [26] and write the effect of the force at some point in the Sun in terms of a function

$$W(r) = \frac{2\pi\lambda}{r} \int_0^{R_{sun}} dr' r' n_e(r') \left(e^{-|r'-r|/\lambda} - e^{-(r'+r)/\lambda} \right), \tag{24}$$

where λ is the range of the force. Long range forces of this kind can be probed by studying experimental tests of the equivalence principle; this sort of analysis was used to get a bound on a vector long-range force's dimensionless coupling constant $k_V < 10^{-49}$ [45]. More recently Gonzalez-Garcia et al [26] performed a two flavor oscillation analysis of solar data to find 3σ bounds for scalar, vector, and tensor forces of infinite range that couple to electron number of

$$k_S(e) \leq 5.0 \times 10^{-45} \text{ (} m_1 = 0\text{eV)}, \tag{25}$$

$$k_S(e) \leq 1.5 \times 10^{-46} \text{ (} m_1 = 0.1\text{eV)}, \tag{26}$$

$$k_V(e) \leq 2.5 \times 10^{-53}, \tag{27}$$

$$k_T(e) \leq 1.7 \times 10^{-60} \text{eV}^{-1}. \tag{28}$$

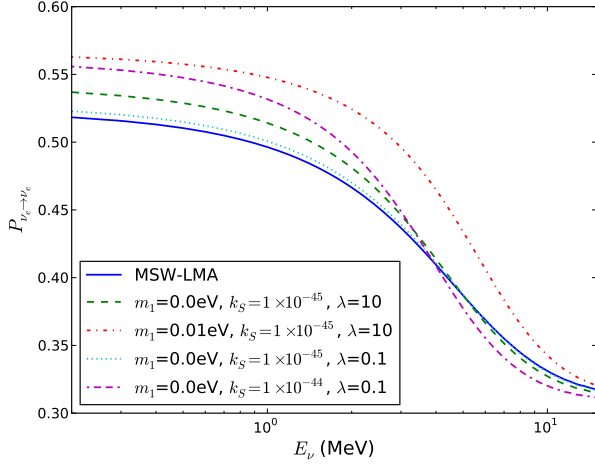


FIG. 7. (Color online) Survival probabilities for a long-range scalar interaction at various values of the range and strength of the coupling and the neutrino mass scale.

1. Scalar Interaction

In the case where the new long-range force is a scalar coupling, we see a similar situation to the MaVaN. We now have a light scalar that only couples to neutrinos and electrons, which one can parameterize in terms of the function $W(r)$. The new term in the Lagrangian for the neutrinos is

$$\mathbf{L} = -g_0 \phi \bar{\nu} \nu \quad (29)$$

and so the kinetic part of the Hamiltonian gains a term

$$\mathbf{M}' = U_{12}^\dagger U_{13}^\dagger U_{23}^\dagger \begin{pmatrix} -M_s(r) & 0 & 0 \\ 0 & 0 & 0 \\ 0 & 0 & 0 \end{pmatrix} U_{23} U_{13} U_{12}, \quad (30)$$

where $M_s(r) = k_s(e)W(r)$ and $k_s(e) = \frac{g_0^2}{4\pi}$. After decoupling the third flavor and diagonalizing the mass matrix for the remaining two we get the matter mixing angle in the adiabatic limit of

$$\sin 2\theta_{12}^m(r_0) = \frac{\sin 2\theta_{12} \Delta m_{12}^2}{\Delta m_s'^2} \quad (31)$$

where

$$\begin{aligned} \Delta m_s'^2 &= \Delta m_{12}^2 - M_s(r_0) \Delta m_{12} c_{13}^2, \\ (\Delta m_s'^2)^2 &= [\Delta m_s^2 \cos 2\theta_{12} - 2E_\nu V(r_0) c_{13}^2 \\ &\quad - M_s^2(r_0) c_{13}^2 + M_s(r_0)(m_1 + m_2)]^2 \\ &\quad + \sin 2\theta_{12} \Delta m_s^2. \end{aligned} \quad (32)$$

The survival probability for various values of the range and coupling strength is shown in Fig. 7.

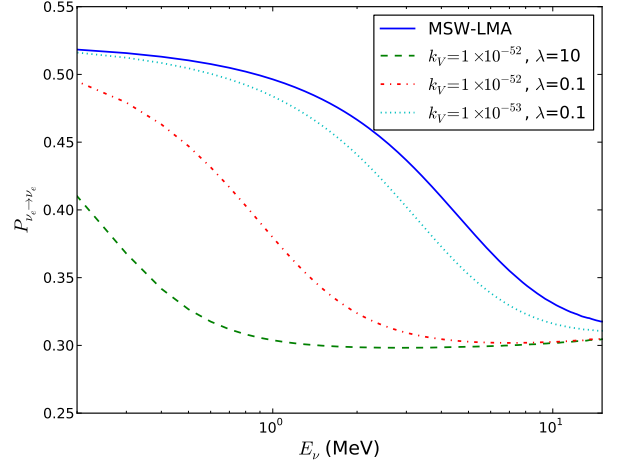


FIG. 8. (Color online) Survival probabilities for a long-range vector interaction at various values of the range and strength of the coupling.

2. Vector Interaction

If the force is mediated by a vector boson A_α , then

$$\mathbf{L} = -g_1 A_\alpha \bar{\nu} \gamma^\alpha \nu \quad (34)$$

and the potential $V(r) = V_{MSW} + k_V W(r)$ where $k_V = \frac{g_1^2}{4\pi}$. We can solve for the survival probability using the standard MSW oscillation equations, substituting in the above for the MSW potential.

The survival probability for various values of the range and coupling strength is shown in Fig. 8.

3. Tensor Interaction

If the force is mediated by a tensor field with spin 2, $\chi_{\alpha\beta}$, then

$$\mathbf{L} = -\frac{g_2}{2} \chi_{\alpha\beta} (\bar{\nu} \gamma^\alpha i \partial^\beta \nu - i \partial^\alpha \bar{\nu} \gamma^\beta \nu). \quad (35)$$

Now the potential is $V(r) = V_{MSW} + E_\nu k_T W(r)$, where $k_T = m_e \frac{g_2^2}{4\pi}$. Again we can use the standard MSW oscillation equations substituting in this new potential.

The survival probability for various values of the range and coupling strength is shown in Fig. 9.

D. Non-Standard Solar Model

We want to check that any improvement in the fit achieved by replacing MSW with a non-standard model cannot be easily reproduced by modifying solar model parameters. In addition, we want to see that we are

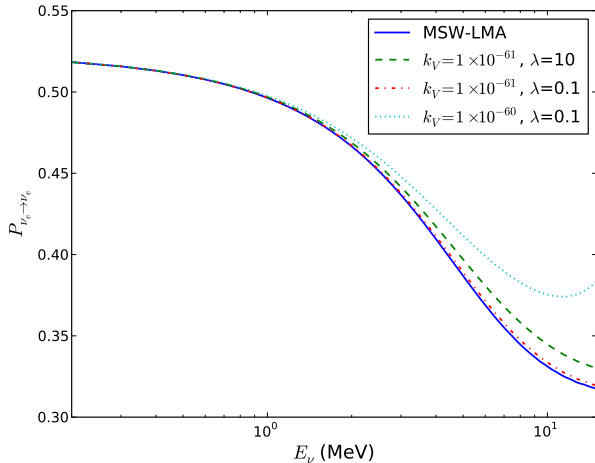


FIG. 9. (Color online) Survival probabilities for a long-range tensor interaction at various values of the range and strength of the coupling.

sensitive to the transition region independent of exact knowledge of the Sun — that is, that small changes in the parameters of the solar model do not create changes in the transition region on the order of the small effects expected from non-standard models. To this end, in addition to comparing fits using both the high metallicity and low metallicity solar models, we use the fact that in the adiabatic approximation, there are only two inputs from the solar model that affect the survival probability. They are the absolute flux constraints, and the convolution of the density profile with the neutrino production profiles. We can effectively remove many of our assumptions about the solar model from our fit by removing the absolute flux constraints entirely, and for the other two sets of parameters, distorting the density profile linearly, so that

$$n'_e(r) = (1 + \delta_0 + \alpha r)n_e(r) \quad (36)$$

for some change in the core density δ_0 , where α is determined by δ_0 and the constraint that the total mass remains the same. A recent study has shown that a change in the central density is plausible, and was able to create a model with the central density increased by over 10% using stellar evolution software [46].

We can get a reasonable constraint on the uncertainty of the solar density profile by comparing the predictions of standard solar models to helioseismological measurements of the sound profile, which differ by around 1% [47, 48].

In this fit we will not constrain the density change since we are also using it as a proxy for any change in the production profile. Additionally, although we cannot use the flux constraints from the solar model in this fit since they are no longer valid once we change the density, we can constrain the sum of the fluxes using the luminosity of the Sun [49] and constrain the ratio of the pp to pep

fluxes since the nuclear matrix elements are the same [50].

IV. RESULTS

A. Large Mixing Angle MSW

We find the best fit point for standard MSW-LMA at $\Delta m_{21}^2 = 7.462 \times 10^{-5} \text{ eV}^2$, $\sin^2 \theta_{12} = 0.301$, $\sin^2 \theta_{13} = 0.0242$, with a ${}^8\text{B}$ flux of $5.31 \times 10^6 \text{ cm}^{-2}\text{s}^{-1}$. The fit compared to the data sets of SNO, Borexino, and S-K is shown in Figs. 10-14. Although in general for the analyses in this paper we marginalize over S-K's systematic uncertainties, it is important to note how they affect the goodness of the fit. To show this effect, we plot the observed rate in S-K against the predicted rate calculated from our best fit mixing parameters in two ways: first fixing the energy scale, energy resolution, and efficiency to the values reported by S-K, and second using values for these parameters obtained by floating them in our fit. In both cases the width of the band does not include any of the systematic uncertainties associated with these parameters since they are energy dependent and so cannot be captured in a single plot. We find the best fit with the energy scale at $+1.1\sigma$, the energy resolution at -1.0σ and the overall efficiency at $+0.6\sigma$. The efficiency systematic uncertainty increases the average predicted ratio while the other two each bend up the high energy end of the spectrum. In other words, while the LMA prediction appears to be a poor fit to the high-energy region of the S-K data, the allowed variation from S-K's systematic uncertainties can explain the difference if they are moved roughly 1σ from their central values. Better constraints on the S-K detector response parameters might therefore lead to a more significant disagreement with the LMA model.

B. Non-Standard Forward Scattering

We formulate our results for this section to be comparable to Palazzo [21], so $\epsilon_{\alpha\beta}^e = \epsilon_{\alpha\beta}^u = 0$. For a more general case to first order n_f/n_e can be considered constant in the Sun, thus any combination of $\epsilon^{e,u,d}$'s would just be a scaling of our results.

First we consider only real ϵ_1 with $\epsilon_2 = 0$. Including the most up-to-date solar results and the most recent KamLAND results as a constraint, letting θ_{12} and Δm_{12}^2 float and fixing $\theta_{13} = 0$, we get a best fit of $\epsilon_1 = -0.137_{-0.071}^{+0.070}$, shown in Fig. 15, which well matches results from Palazzo. After letting θ_{13} float and adding in the constraint from RENO and Daya Bay, the significance becomes smaller, with a best fit value of $\epsilon_1 = -0.145_{-0.109}^{+0.118}$, shown in Figs. 16 and 17. The best fit survival probability compared to MSW-LMA and to data considered in this analysis is shown in the appendix in Fig. 27.

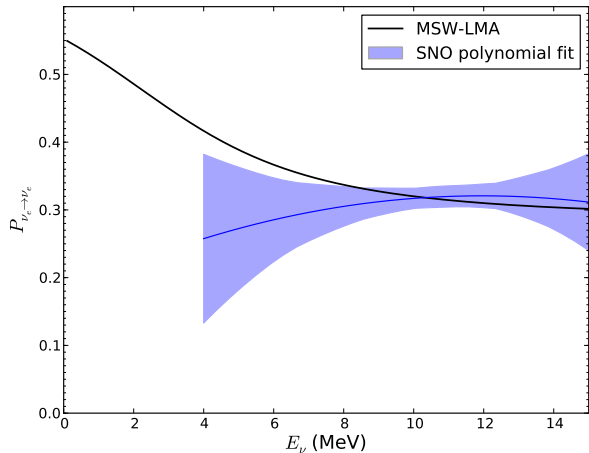


FIG. 10. (Color online) Our best fit MSW-LMA prediction versus SNO extracted ${}^8\text{B}$ survival probability. The band represents the RMS spread at any given energy, i.e., not including energy correlations.

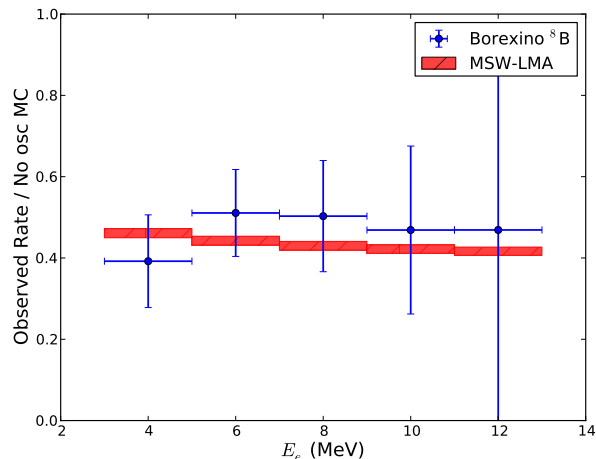


FIG. 11. (Color online) Borexino event rate binned in measured electron energy with each bin scaled by Monte Carlo predictions assuming GS98SF2 fluxes, versus the same ratio for the expected rates assuming our best fit LMA parameters and fluxes. Error bars on the data points represent statistical uncertainties only. The best fit oscillation prediction band width represents the uncertainty on the ${}^8\text{B}$ flux.

These results seem to allow a vacuum to matter transition in the survival probability at higher energies than the SNO data suggests. It is important to consider the fit to the day night asymmetry, shown in Fig. 18 for SNO. The NSI does not have a large effect on the asymmetry, and so for both models the best fit does not fit the data well. The correlations between the asymmetry and the day survival probability translate this poor fit to an even broader allowed upturn, further limiting the significance of any flatness in the data. We show this effect by fitting

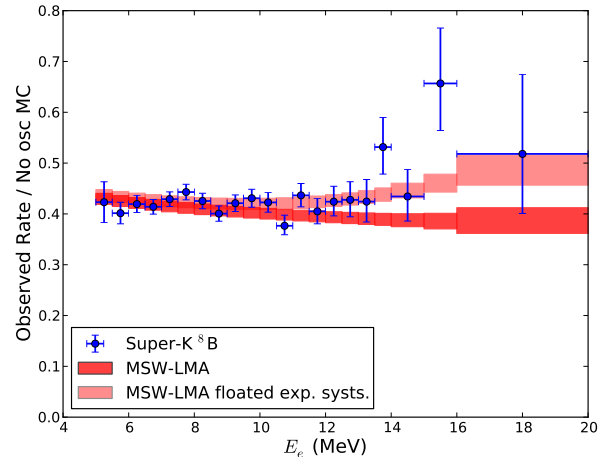


FIG. 12. (Color online) S-K I event rates binned in measured electron energy with each bin scaled by Monte Carlo predictions assuming GS98SF2 fluxes, versus the same ratio for the expected rates assuming our combined best fit LMA parameters and fluxes. Error bars on the data points represent statistical and energy uncorrelated systematic uncertainties combined in quadrature. The two bands show the effect of the correlated systematic uncertainties: for the dark band, detector response parameters have been fixed at their reported values, while for the light they have been floated in the fit. The best fit oscillation prediction band width represents the uncertainty on the ${}^8\text{B}$ flux.

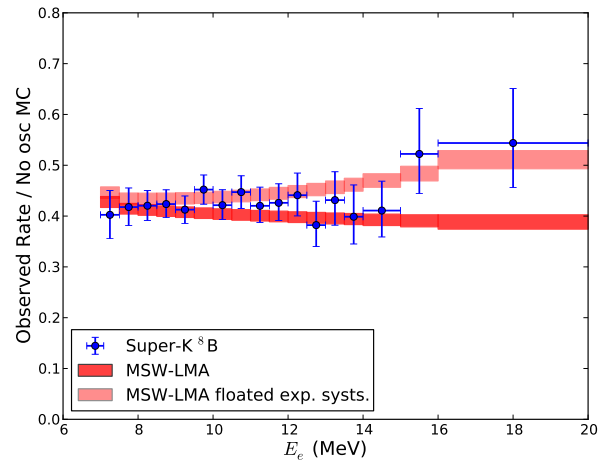


FIG. 13. (Color online) S-K II event rates binned in measured electron energy with each bin scaled by Monte Carlo predictions assuming GS98SF2 fluxes, versus the same ratio for the expected rates assuming our combined best fit LMA parameters and fluxes. Error bars on the data points represent statistical and energy uncorrelated systematic uncertainties combined in quadrature. The two bands show the effect of the correlated systematic uncertainties: for the dark band, detector response parameters have been fixed at their reported values, while for the light they have been floated in the fit. The best fit oscillation prediction band width represents the uncertainty on the ${}^8\text{B}$ flux.

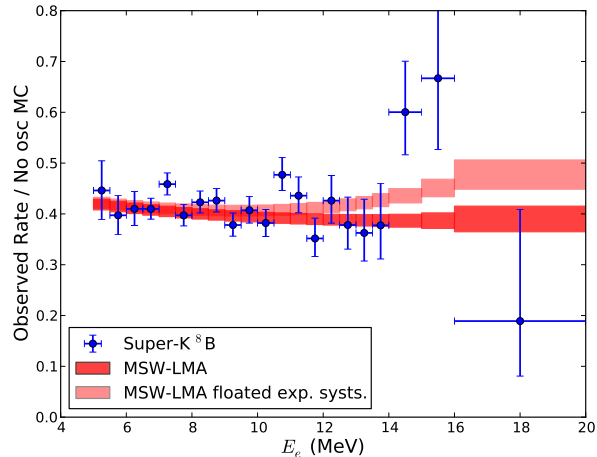


FIG. 14. (Color online) S-K III event rates binned in measured electron energy with each bin scaled by Monte Carlo predictions assuming GS98SF2 fluxes, versus the same ratio for the expected rates assuming our combined best fit LMA parameters and fluxes. Error bars on the data points represent statistical and energy uncorrelated systematic uncertainties combined in quadrature. The two bands show the effect of the correlated systematic uncertainties: for the dark band, detector response parameters have been fixed at their reported values, while for the light they have been floated in the fit. The best fit oscillation prediction band width represents the uncertainty on the ^8B flux.

the MSW-LMA predicted day-night asymmetry to Eq. 2 and then recalculating what the RMS spread in the day night survival probability would be after fixing a_0 and a_1 given the correlation matrix, as shown in 19.

In addition, since these plots scale the absolute rates to get survival probabilities, they hide the relationship between the survival probability and the absolute flux. Both of these effects can be seen more clearly in the correlation matrix for SNO's polynomial survival probability fit, Table VIII in Ref. [29]. The baseline level of the survival probability c_0 is strongly anticorrelated with the absolute flux Φ_B , and the slope of the survival probability c_1 is anticorrelated with the slope of the day night asymmetry a_1 .

To better visualize why the full fit does not have a better constraint, we applied the polynomial survival probability fit as used for the SNO data to the combination of the SNO, S-K, Borexino, and Homestake results. This represents a fit to the survival probability independent of any physics model, where the polynomial forms in Eqs. 1 and 2 are used to impose an energy correlation under the model independent assumption that there is no small scale structure to the survival probability. Since the Homestake results could contain a significant fraction of non- ^8B events, one additional term for the average non- ^8B survival probability is added to the fit, where non- ^8B fluxes were fixed at SSM values. The results of the fit are given in Tables I and II, and the best fit and RMS spread

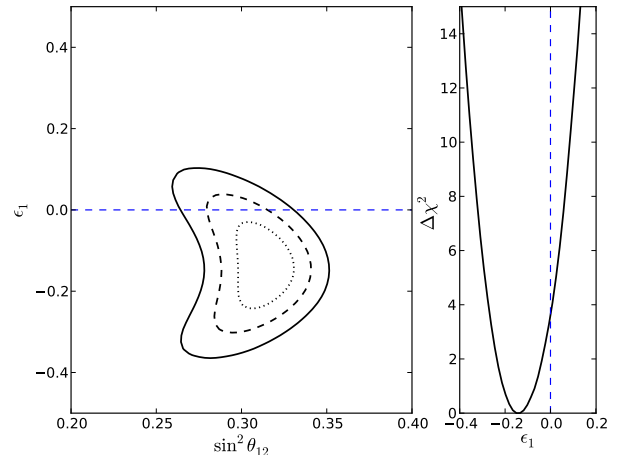


FIG. 15. Left: Two flavor contours with $\epsilon_2 = 0$ and real ϵ_1 . Contours are shown for 68%, 95%, and 99.73% confidence levels for 2 d.o.f., where the χ^2 has been minimized with respect to all undisplayed parameters. Right: $\Delta\chi^2$ as a function of ϵ_1 .

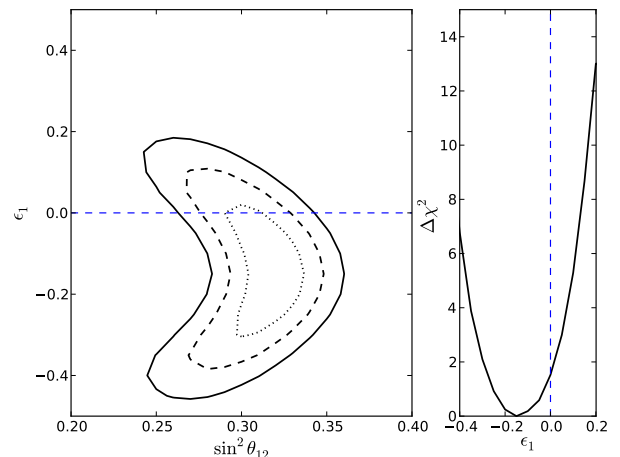


FIG. 16. Left: Three flavor contours including constraints from RENO and Daya Bay. Contours are shown for 68%, 95%, and 99.73% confidence levels for 2 d.o.f., where the χ^2 has been minimized with respect to all undisplayed parameters. Right: $\Delta\chi^2$ as a function of ϵ_1 .

is shown in Fig. 20. The majority of the change from the SNO-only band is driven by the S-K results, where the high-energy end and the ^8B flux is pulled upward. Although their data looks flat in detected energy, when projected back into incident neutrino energy it becomes consistent with an LMA-like transition, as suggested in Figs. 12, 13, and 14. The band of the RMS spread shows the significance to which we can say anything about the shape of the survival probability at low energies, and we can see that the band covers the MSW-LMA prediction but at the same time allows for a perfectly flat or

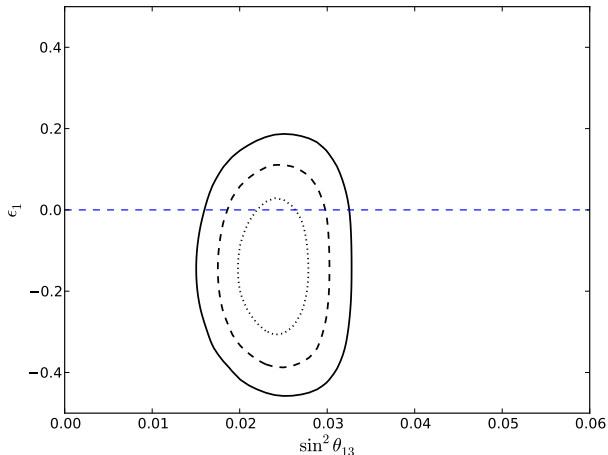


FIG. 17. Three flavor contours including constraints from RENO and Daya Bay for ϵ_1 and θ_{13} . Contours are shown for 68%, 95%, and 99.73% confidence levels for 2 d.o.f., where the χ^2 has been minimized with respect to all undisplayed parameters.

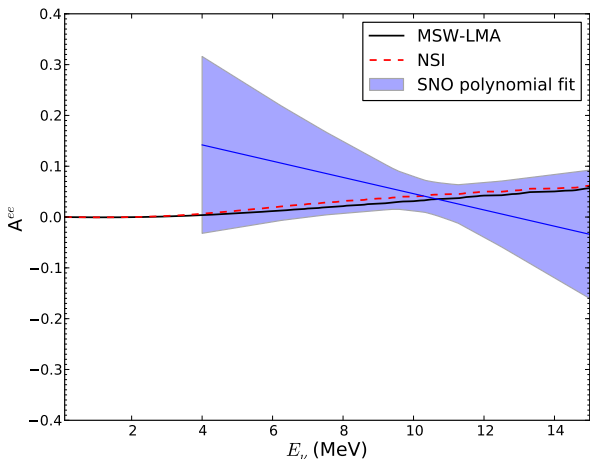


FIG. 18. (Color online) Day-Night asymmetry from SNO results compared to best fit MSW-LMA and NSI. The band represents the RMS spread at any given energy, i.e., not including energy correlations.

even downward bending survival probability. Note that this combined polynomial fit does not impact any of the results in this paper since we are only using it to visualize the survival probability and do not actually use it in our likelihood fits.

We also consider the case of complex ϵ_1 . Here the best fit is found at $\epsilon_1 = -0.146 + 0.031i$. The fit results are shown in Fig. 21 and the best fit survival probability in the appendix in Fig. 28. For both ϵ_1 and ϵ_2 nonzero, we find the best fit point at $\epsilon_1 = 0.014, \epsilon_2 = 0.683$. The fit contours are shown in Fig. 22, and the best fit survival

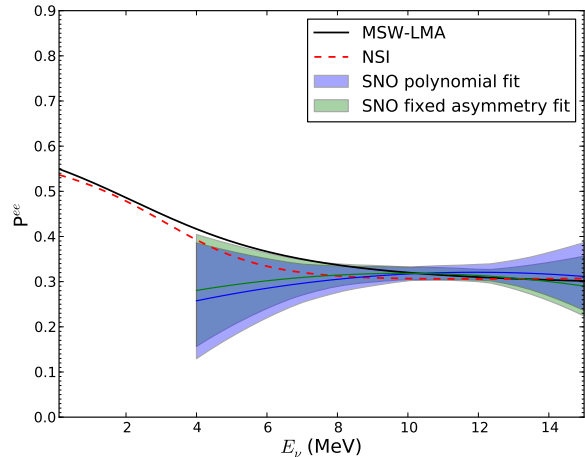


FIG. 19. (Color) Day survival probability for SNO. The blue band shows the RMS spread from the best fit, and the green band shows the spread after the Day-Night asymmetry is fixed to the MSW-LMA prediction.

	Best Fit	Fit Error
Φ_B	5.403	0.195
c_0	0.309	0.015
c_1	-0.0014	0.0055
c_2	0.008	0.0022
a_0	0.047	0.020
a_1	0.000	0.018
$P_{\text{non-}s_B}$	0.393	0.148

TABLE I. Results for polynomial fit for the survival probability and day-night asymmetry fit to the data of SNO, S-K, Borexino, and Homestake.

probability is shown in Fig. 29. In both cases the additional free parameter allows a slightly better fit, but the standard MSW-LMA is within the 68% confidence interval for two degrees of freedom. Once both ϵ_1 and ϵ_2 are allowed to be nonzero, there is no further improvement in the fit if we again let ϵ_1 be complex.

	Φ_B	c_0	c_1	c_2	a_0	a_1	$P_{\text{non-}s_B}$
Φ_B	1.000	-0.793	0.215	-0.152	-0.027	0.016	0.045
c_0	-0.793	1.000	-0.289	-0.279	-0.204	-0.009	-0.074
c_1	0.215	-0.289	1.000	-0.010	0.042	-0.587	0.023
c_2	-0.152	-0.279	-0.010	1.000	-0.032	-0.004	-0.073
a_0	-0.027	-0.204	0.042	-0.032	1.000	-0.073	0.014
a_1	0.016	-0.009	-0.587	-0.004	-0.073	1.000	0.005
$P_{\text{non-}s_B}$	0.045	-0.074	0.023	-0.073	0.014	0.005	1.000

TABLE II. Correlation matrix from the polynomial fit for the survival probability and day-night asymmetry fit to the data of SNO, S-K, Borexino, and Homestake.

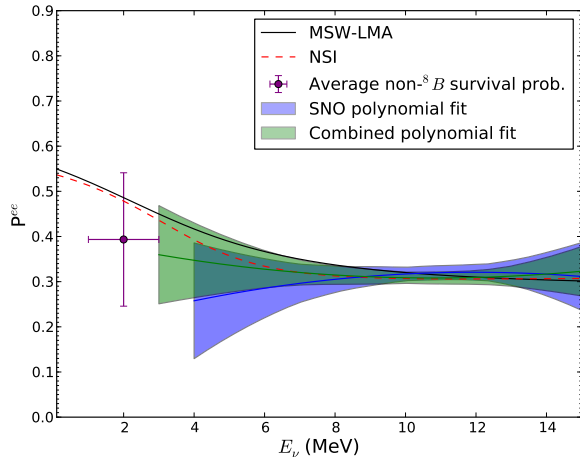


FIG. 20. (Color) Polynomial fit to SNO, Super-Kamiokande, Borexino ${}^8\text{B}$ data and Homestake's results. The band represents the RMS spread at any given energy, i.e., not including energy correlations.

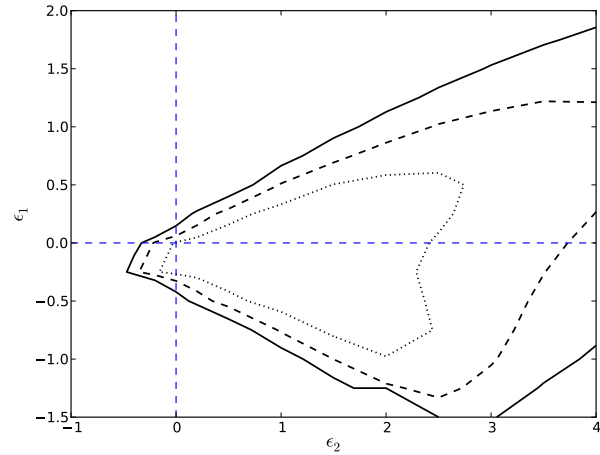


FIG. 22. Results for NSI fit with real ϵ_1 . Contours are shown for 68%, 95%, and 99.73% confidence levels (2 d.o.f.), where the χ^2 has been minimized with respect to all undisplayed parameters.

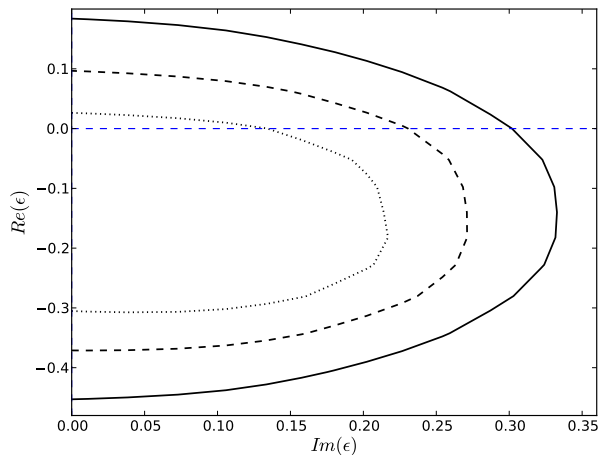


FIG. 21. Results for NSI fit with $\epsilon_2 = 0$ but complex ϵ_1 . Contours are shown for 68%, 95%, and 99.73% confidence levels (2 d.o.f.), where the χ^2 has been minimized with respect to all undisplayed parameters.

For all of these scenarios, the best fit values for the non-standard parameters ϵ_1 and ϵ_2 are well within the current experimental bounds. At the same time, they represent relatively substantial effects, considering that at $\epsilon_{\alpha\beta} = 1$ the non-standard interaction has the same strength as the MSW potential, as shown in Eq. 4.

C. Mass Varying Neutrinos

1. Neutrino Density Effects

After fitting for $m_{1,0}$ letting all mixing parameters float, we found that the best fit point was at $m_{1,0} = 0$, where this model's predictions become identical to MSW-LMA. Our fit results, as shown in Fig. 23, give a 90% confidence level upper limit on the neutrino mass scale of $m_{1,0} < 0.033\text{eV}$ within this model. Our results do not agree with the previous limit in [23], who found a limit an order of magnitude smaller. We cannot explain the difference, although they use older data sets for each experiment. For the inverted hierarchy we expect $m_{1,0} \gtrsim \sqrt{\Delta m_{atm}^2} \sim 0.05\text{ eV}$, so within the context of this model, the inverted hierarchy would be rejected.

2. Fermion Density Effects

For simplification we let $m_{1,0} = \alpha_1 = 0$, so we fit for $\alpha_2, \text{Re}[\alpha_3], \text{Im}[\alpha_3]$. Results for $\alpha_2 > 0, \alpha_3^2 < 0$ are shown in Fig. 24. In this case our best fit is at $\alpha_2 = 5.95 \times 10^{-5}$, $\alpha_3 = i1.97 \times 10^{-5}$, shown in the appendix in Fig. 30, although the 2σ contour includes the origin. Note that although the ${}^8\text{B}$ survival probability in Fig. 30 seems to be far from the Borexino pep point, in this scenario the pep survival probability is actually significantly different than ${}^8\text{B}$'s at the same energy, making it more consistent with the data than it would appear. Minimizing over all other variables gives the bounds at 90% confidence for 1 d.o.f. of

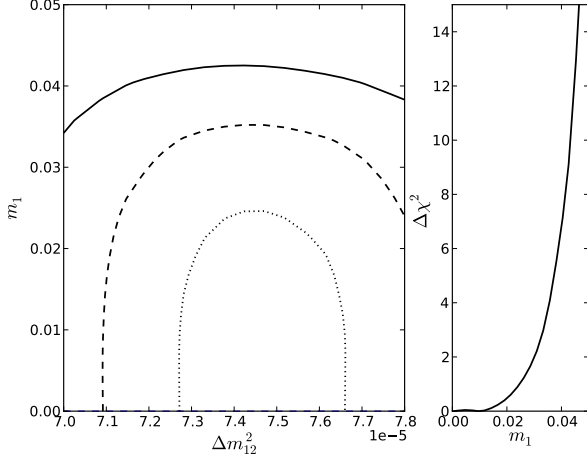


FIG. 23. Results for MaVaN model with neutrino mass coupled to neutrino density. Left: Contours are shown for 68%, 95%, and 99.73% confidence levels for 2 d.o.f., where the χ^2 has been minimized with respect to all undisplayed parameters. Right: $\Delta\chi^2$ as a function of $m_{1,0}$.

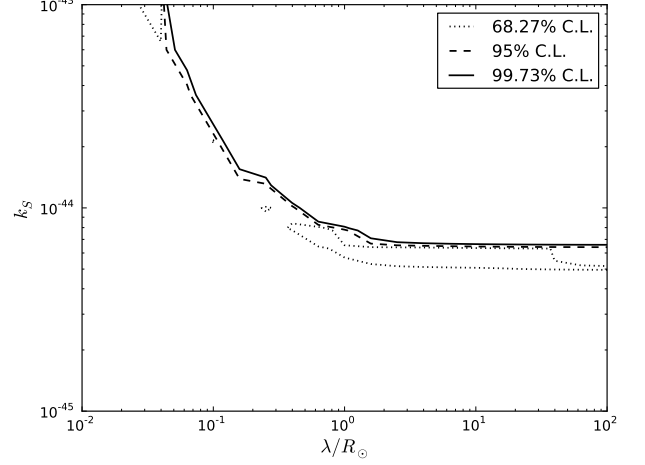


FIG. 25. Results for MaVaN model with a scalar long-range force and $m_{1,0} = 0$. Contours are shown for 68%, 95%, and 99.73% confidence levels (2 d.o.f.), where the χ^2 has been minimized with respect to all undisplayed parameters.

D. Long-Range Leptonic Forces

For the scalar long-range leptonic force, we find that after again fixing $m_{1,0} = 0$, the best fit is at $k_S = 6.73 \times 10^{-45}$, $\lambda = 1.56R_\odot$. Since $\lambda = 1/m_S$, this point represents a force mediated by a scalar particle with mass $m_S = 9.1 \times 10^{-17}\text{eV}$ and a coupling strength $g_0 = 2.91 \times 10^{-22}$. The best fit survival probability is shown in the appendix in Fig. 31. Like the MaVaN case, the *pep* survival probability is higher than ^8B 's at the same energy. For the long-range vector force, we find the best fit at $k_V = 3.26 \times 10^{-54}$, $\lambda = 16.97R_\odot$, shown in Fig. 32. For the tensor long-range force, there is no improvement of the fit to the data and the best fit remains at MSW-LMA.

In all three cases, standard MSW-LMA is within the 1σ contour, but the constraint on the coupling strength gets stronger as λ increases. The contours for the scalar case are shown in Fig. 25. At $\lambda = \infty$, we can set upper limits on the coupling strengths at 90% confidence level for 1 d.o.f. of

$$k_S(e) \leq 6.31 \times 10^{-45} \text{ with } m_1 = 0\text{eV}, \quad (40)$$

$$k_V(e) \leq 1.23 \times 10^{-53}, \quad (41)$$

$$k_T(e) \leq 1.31 \times 10^{-61}\text{eV}^{-1}. \quad (42)$$

E. Non-Standard Solar Model

We found that using the low metallicity (AGSS09SF2) solar model's flux constraints and solar distributions did not give noticeably different results, and in general worsened the fits for any model.

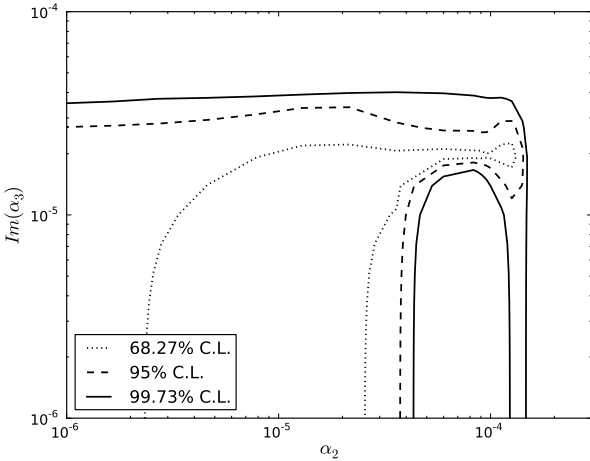


FIG. 24. Results for MaVaN model with neutrino mass coupled to fermion density with $\alpha_2 > 0$ and $\alpha_3 < 0$. Contours are shown for 68%, 95%, and 99.73% confidence levels (2 d.o.f.), where the χ^2 has been minimized with respect to all undisplayed parameters.

$$1.6 \times 10^{-6} \leq \alpha_2/\text{eV} \leq 1.3 \times 10^{-4}, \quad (37)$$

$$|\alpha_3|/\text{eV} \leq 2.48 \times 10^{-5} \text{ for } \alpha_3^2 > 0, \quad (38)$$

$$|\alpha_3|/\text{eV} \leq 2.29 \times 10^{-5} \text{ for } \alpha_3^2 < 0. \quad (39)$$

Then from Eq. 16, we can use our limits on the parameters to get a combined limit on the couplings of $|\lambda^{ij}\lambda^N|/m_\phi^2 \leq 2.8 \times 10^{-14}\text{eV}^{-2}$ [24].

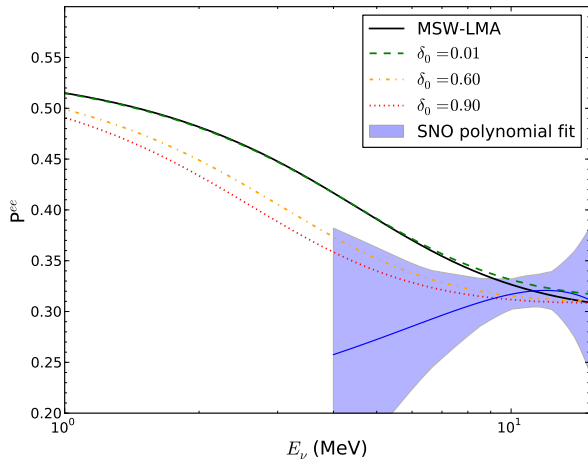


FIG. 26. (Color online) Survival probability for MSW-LMA with various fractional increases δ_0 of the solar core density compared to the SNO results.

As described in Section III D, we looked at the effect of changing the density of the solar core to see whether we are susceptible to mistaking a small difference in the expected solar model for a non-standard interaction. Fig. 26 shows the survival probability with the core density increased by various amounts. It is clear that within the range suggested by helioseismological measurements of about 1%, the change in the ${}^8\text{B}$ upturn is not large enough to mimic any of the non-standard models. Fitting for the central density while keeping the rest of the fit the same, we find that the improvement in the fit for a change of up to 1% is marginal, and we don't reach a minimum until an implausible increase in the solar core density of around 90%. Since any change in the central density would change the core temperature and thus also the expected fluxes, we fit again allowing the density to float and replacing the flux constraints from the solar model with an overall luminosity constraint and a constraint on the pp to pep ratio. Here the best fit is found at an increase of 57%, with a $\Delta\chi^2$ of -4.6 , although not changing the density and just removing the flux constraints already gives a $\Delta\chi^2$ of -3.5 .

V. CONCLUSIONS

We have compared the predictions of survival probabilities for several models of neutrino non-standard interactions compared to standard MSW-LMA oscillations using results from solar experiments constrained by terrestrial measurements of the mixing parameters. The results of the fits are summarized in Table III.

Although several of these models allow for a better fit

to the data and suggest an explanation for the flatness of the ${}^8\text{B}$ survival probability, we have shown that with the current available data on solar neutrino interactions, there is no model that has demonstrated to be better than MSW-LMA with greater than 2σ significance. We have found that the low significance is in part due to the known, large value of θ_{13} , but also because of the as-yet large systematic uncertainties and covariances in the experimental data sets. The critical transition region thus remains largely unexplored.

We have also examined whether small changes to the solar density profile could lead to a change in the transition region that could mimic the effects of new physics. The results of our simple model show that in fact this is not the case. The matter/vacuum transition region is therefore a good place to look for small effects of non-standard models.

Our best fit survival probabilities show that because most of our non-standard model effects have a solar radial or density dependence, the effect is lessened in the pep or pp production regions and so it would be difficult to test these models merely by improving the measurement of either of those signals. It would require either a better measurement of lower energy ${}^8\text{B}$, especially one with a charged-current interaction that preserves more of the spectral information, or a new model that can more closely match the data in order for this discrepancy to become more than a hint of something non-standard.

To fully probe this interesting region, in which the interferometry provided by neutrino oscillations lets us look for even tiny effects of new physics, will require new experiments or more precisely constrained systematic uncertainties. Both the Super-Kamiokande and Borexino experiments will continue to take data and hopefully their uncertainties will continue to improve. The SNO+ experiment will begin taking data in the near future and it, too, will be able to probe this region. It is possible, however, that a measurement using a charged-current reaction, which preserves more of the spectral information, may be necessary to provide the needed precision to see any new physics that may lie in this region.

ACKNOWLEDGMENTS

We would like to thank the SNO collaboration for their helpful comments and for allowing us to spot check our code against theirs, and in particular Nuno Barros for many helpful suggestions. We also would like to thank Aldo Serenelli for providing us with information on the solar models used in this paper, Stefano Davini for details on Borexino's pep results, and Alex Friedland and Michael Smy for helpful and interesting conversations. This work has been supported by the US Department of Energy, Office of Nuclear Physics, the University of California at Berkeley, and Lawrence Berkeley National Laboratory.

Model	Best Fit	$\Delta\chi^2$	Additional D.o.F.	C.L.
MSW-LMA	$\Delta m_{21}^2 = 7.462 \times 10^{-5} \text{ eV}^2, \sin^2 \theta_{12} = 0.301,$ $\sin^2 \theta_{13} = 0.0242$	0	—	—
MSW-LMA (AGSS09SF2)	$\Delta m_{21}^2 = 7.469 \times 10^{-5} \text{ eV}^2, \sin^2 \theta_{12} = 0.304,$ $\sin^2 \theta_{13} = 0.0240$	2.8	—	—
NSI (ϵ_1 real, $\epsilon_2 = 0$)	$\epsilon_1 = -0.145$	-1.5	1	0.78
NSI ($\epsilon_2 = 0$)	$\epsilon_1 = -0.146 + 0.031i$	-1.5	2	0.53
NSI (ϵ_1 real)	$\epsilon_1 = 0.014, \epsilon_2 = 0.683$	-1.9	2	0.60
MaVaN neutrino density dependence	$m_{1,0} < 0.033 \text{ eV}$	0	1	0.0
MaVaN fermi density dependence	$\alpha_2 = 5.95 \times 10^{-5}, \alpha_3 = i1.97 \times 10^{-5}$	-3.4	2	0.81
Long range scalar leptonic force	$k_S = 6.73 \times 10^{-45}, \lambda = 1.56 R_\odot, m_{1,0} = 0 \text{ eV}$	-2.9	3	0.58
Long range vector leptonic force	$k_V = 3.26 \times 10^{-54}, \lambda = 16.97 R_\odot$	-1.8	2	0.59
Long range tensor leptonic force	$k_T < 1.3 \times 10^{-61} \text{ eV}^{-1}$	0	2	0.0
Non-standard solar model	$\delta_0 = 0.57$	-4.6	1	—
without flux constraint				

TABLE III. Comparison of survival probability fits to standard MSW-LMA. If the best fit remains at the MSW-LMA value for a model, a 90% confidence level upper limit (1 d.o.f.) on the model's parameters is given instead. $\Delta\chi^2$ is the difference between the model's best fit point and the MSW-LMA best fit. The final column gives the largest confidence level at which MSW-LMA is excluded.

- [1] J. K. Ahn *et al.* (RENO Collaboration), (2012), arXiv:1204.0626 [hep-ex].
- [2] F. P. An *et al.* (Daya Bay Collaboration), Chinese Physics C **37**, 011001 (2013).
- [3] A. Aguilar *et al.* ((LSND Collaboration)), Phys. Rev. D **64**, 112007 (2001).
- [4] A. A. Aguilar-Arevalo *et al.* (MiniBooNE Collaboration), Phys. Rev. Lett. **105**, 181801 (2010).
- [5] P. Adamson *et al.* (MINOS Collaboration), Phys. Rev. Lett. **107**, 011802 (2011).
- [6] S. N. Gninenko, Phys. Rev. Lett. **103**, 241802 (2009).
- [7] V. Barger, J. Learned, P. Lipari, M. Lusignoli, S. Pakvasa, and T. Weiler, Physics Letters B **462**, 109 (1999).
- [8] L. Wolfenstein, Phys. Rev. D **17**, 2369 (1978).
- [9] S. Mikheyev and A. Smirnov, Il Nuovo Cimento C **9**, 17 (1986).
- [10] B. Aharmim *et al.* (SNO Collaboration), Phys. Rev. C **81**, 055504 (2010).
- [11] Y. Abe *et al.* (Double Chooz Collaboration), Phys. Rev. D **86**, 052008 (2012).
- [12] T. Akiri *et al.* (LBNE Collaboration), (2011), arXiv:1110.6249 [hep-ex].
- [13] J. Kisiel *et al.* (LAGUNA Collaboration), PoS **EPS-HEP2009**, 283 (2009).
- [14] K. Abe, T. Abe, H. Aihara, Y. Fukuda, Y. Hayato, *et al.*, (2011), arXiv:1109.3262 [hep-ex].
- [15] A. Gando *et al.* (The KamLAND Collaboration), Phys. Rev. D **83**, 052002 (2011).
- [16] J. N. Bahcall and C. Peña-Garay, New J.Phys. **6**, 63 (2004), arXiv:hep-ph/0404061 [hep-ph].
- [17] A. Friedland, Nucl.Phys.Proc.Suppl. **221**, 79 (2011), arXiv:hep-ph/0612266 [hep-ph].
- [18] A. Friedland, C. Lunardini, and C. Peña-Garay, Physics Letters B **594**, 347 (2004).
- [19] M. Guzzo, P. de Holanda, M. Maltoni, H. Nunokawa, M. Trtola, and J. Valle, Nuclear Physics B **629**, 479 (2002).
- [20] O. G. Miranda, M. A. Trtola, and J. W. F. Valle, Journal of High Energy Physics **2006**, 008 (2006).
- [21] A. Palazzo, Phys. Rev. D **83**, 101701 (2011).
- [22] V. Barger, P. Huber, and D. Marfatia, Phys. Rev. Lett. **95**, 211802 (2005).
- [23] M. Cirelli, M. Gonzalez-Garcia, and C. Peña-Garay, Nuclear Physics B **719**, 219 (2005).
- [24] M. C. Gonzalez-Garcia, P. C. de Holanda, and R. Zukanovich Funchal, Phys. Rev. D **73**, 033008 (2006).
- [25] M. Gonzalez-Garcia and M. Maltoni, Physics Reports **460**, 1 (2008).
- [26] M. C. Gonzalez-Garcia, P. C. de Holanda, E. Mass, and R. Z. Funchal, Journal of Cosmology and Astroparticle Physics **2007**, 005 (2007).
- [27] J. N. Abdurashitov *et al.* (SAGE Collaboration), Phys. Rev. C **80**, 015807 (2009).
- [28] B. T. Cleveland, T. Daily, J. Raymond Davis, J. R. Distel, K. Lande, C. K. Lee, P. S. Wildenhain, and J. Ullman, The Astrophysical Journal **496**, 505 (1998).
- [29] B. Aharmim *et al.* (SNO Collaboration), (2011), arXiv:1109.0763 [nucl-ex].
- [30] J. Hosaka *et al.* (Super-Kamiokande Collaboration), Phys. Rev. D **73**, 112001 (2006).
- [31] J. P. Cravens *et al.* (The Super-Kamiokande Collaboration), Phys. Rev. D **78**, 032002 (2008).
- [32] K. Abe *et al.* (Super-Kamiokande Collaboration), Phys. Rev. D **83**, 052010 (2011).
- [33] G. Bellini *et al.* (Borexino Collaboration), Phys. Rev. Lett. **107**, 141302 (2011).
- [34] G. Bellini *et al.* (Borexino Collaboration), Phys. Rev. D **82**, 033006 (2010).
- [35] G. Bellini *et al.* (Borexino Collaboration), Phys. Rev. Lett. **108**, 051302 (2012).

- [36] S. J. Parke, Phys. Rev. Lett. **57**, 1275 (1986).
- [37] N. Grevesse and A. Sauval, Space Science Reviews **85**, 161 (1998).
- [38] M. Asplund, N. Grevesse, A. J. Sauval, and P. Scott, Ann. Rev. Astron. Astrophys. **47**, 481 (2009).
- [39] A. M. Serenelli, W. Haxton, and C. Peña-Garay, Astrophys.J. **743**, 24 (2011), arXiv:1104.1639 [astro-ph.SR].
- [40] E. K. Akhmedov, M. Tortola, and J. Valle, JHEP **0405**, 057 (2004), arXiv:hep-ph/0404083 [hep-ph].
- [41] E. Lisi and D. Montanino, Phys. Rev. D **56**, 1792 (1997).
- [42] J. N. Bahcall, E. Lisi, D. E. Alburger, L. De Braekeleer, S. J. Freedman, and J. Napolitano, Phys. Rev. C **54**, 411 (1996).
- [43] J. N. Bahcall, Phys. Rev. C **56**, 3391 (1997).
- [44] J. N. Bahcall, M. Kamionkowski, and A. Sirlin, Phys. Rev. D **51**, 6146 (1995).
- [45] L. Okun, Physics Letters B **382**, 389 (1996).
- [46] I. Lopes and S. Turck-Chize, Astrophys.J. **765**, 14 (2013), arXiv:1302.2791 [astro-ph.SR].
- [47] J. N. Bahcall, A. M. Serenelli, and S. Basu, The Astrophysical Journal Supplement Series **165**, 400 (2006).
- [48] J. N. Bahcall, S. Basu, M. Pinsonneault, and A. M. Serenelli, The Astrophysical Journal **618**, 1049 (2005).
- [49] J. N. Bahcall, Phys. Rev. C **65**, 025801 (2002).
- [50] M. Gonzalez-Garcia, M. Maltoni, and J. Salvado, Journal of High Energy Physics **2010**, 1 (2010).

Appendix: Survival Probability Fits

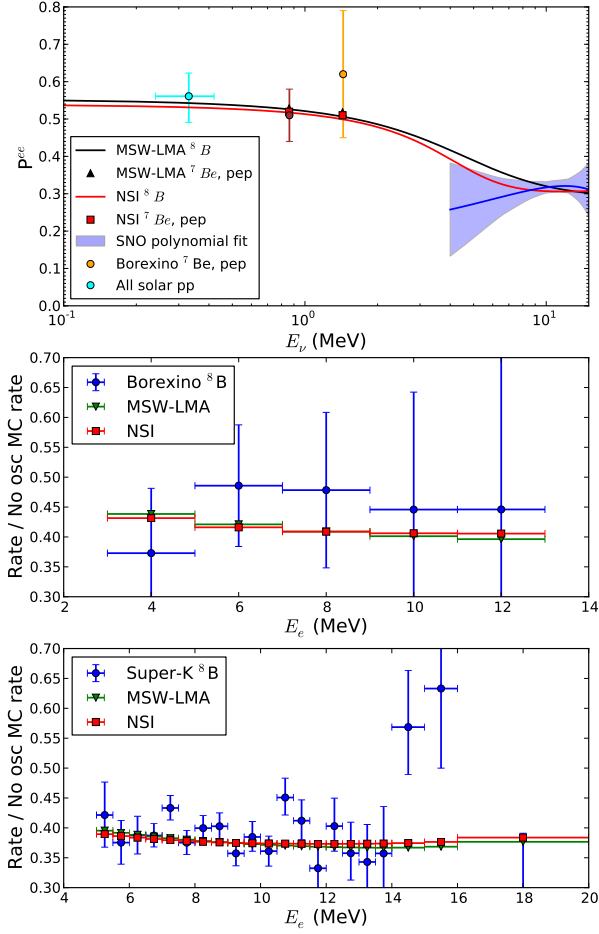


FIG. 27. (Color online) Three flavor best fit NSI survival probability compared to MSW-LMA at $\epsilon_1 = -0.145$, $\Delta m_{21}^2 = 7.481 \times 10^{-5} \text{eV}^2$, $\sin^2 \theta_{12} = 0.320$, $\sin^2 \theta_{13} = 0.0238$. The top plot shows the survival probability as a function of incident neutrino energy. The middle shows the best fit's predicted event rate in Borexino for each of Borexino's measured electron energy bins scaled by the GS98SF2 flux no-oscillation prediction compared to Borexino's data, and the bottom shows the same for S-K III's energy bins and data.

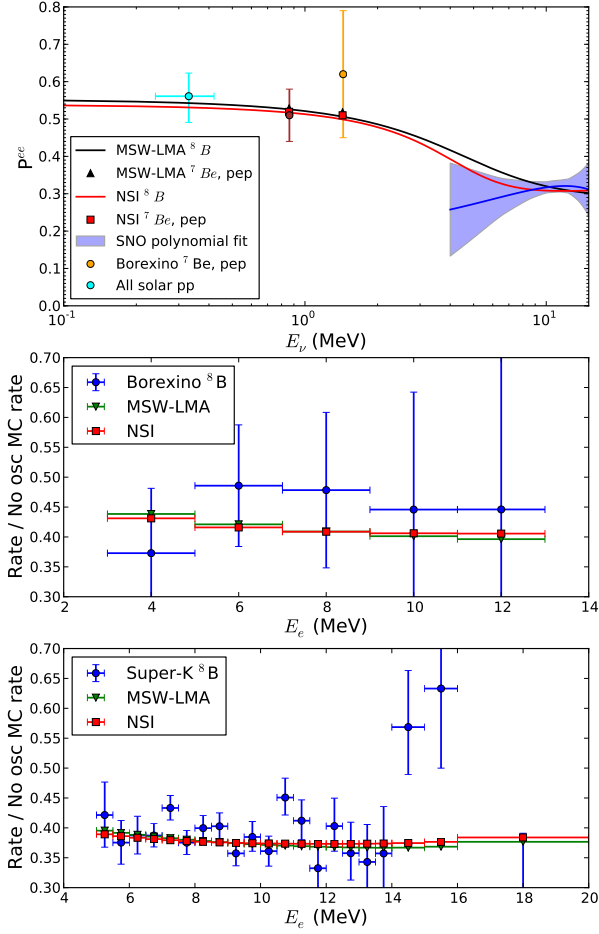


FIG. 28. (Color online) Best fit for NSI fit with $\epsilon_2 = 0$ but complex ϵ_1 at $\epsilon_1 = -0.146 + 0.31i$, $\Delta m_{21}^2 = 7.472 \times 10^{-5} \text{eV}^2$, $\sin^2 \theta_{12} = 0.320$, $\sin^2 \theta_{13} = 0.0238$. The top plot shows the survival probability as a function of incident neutrino energy. The middle shows the best fit's predicted event rate in Borexino for each of Borexino's measured electron energy bins scaled by the GS98SF2 flux no-oscillation prediction compared to Borexino's data, and the bottom shows the same for S-K III's energy bins and data.

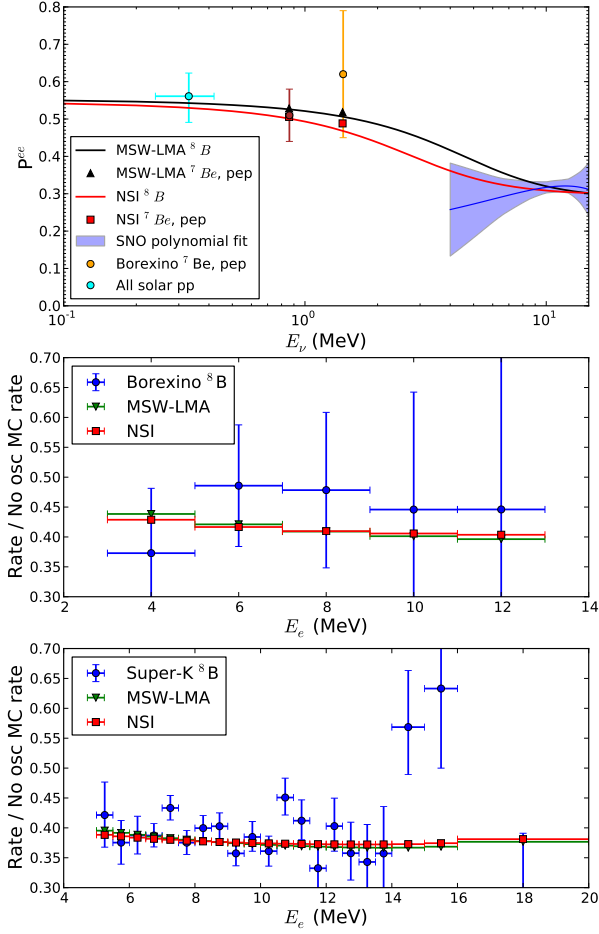


FIG. 29. (Color online) Best fit for NSI fit with real ϵ_1 at $\epsilon_1 = 0.014$, $\epsilon_2 = 0.683$, $\Delta m_{21}^2 = 7.487 \times 10^{-5} \text{eV}^2$, $\sin^2 \theta_{12} = 0.310$, $\sin^2 \theta_{13} = 0.0238$. The top plot shows the survival probability as a function of incident neutrino energy. The middle shows the best fit's predicted event rate in Borexino for each of Borexino's measured electron energy bins scaled by the GS98SF2 flux no-oscillation prediction compared to Borexino's data, and the bottom shows the same for S-K III's energy bins and data.

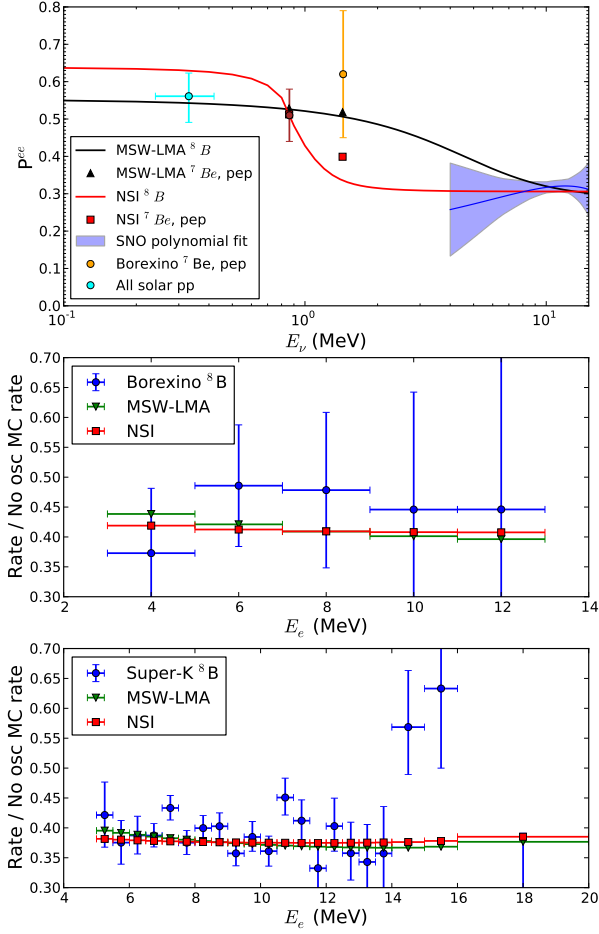


FIG. 30. (Color online) Best fit for fermion density dependent MaVaN at $\alpha_2 = 5.95 \times 10^{-5}$, $\alpha_3 = i1.97 \times 10^{-5}$, $\Delta m_{21}^2 = 7.484 \times 10^{-5} \text{eV}^2$, $\sin^2 \theta_{12} = 0.320$, $\sin^2 \theta_{13} = 0.0239$. The top plot shows the survival probability as a function of incident neutrino energy. The middle shows the best fit's predicted event rate in Borexino for each of Borexino's measured electron energy bins scaled by the GS98SF2 flux no-oscillation prediction compared to Borexino's data, and the bottom shows the same for S-K III's energy bins and data.

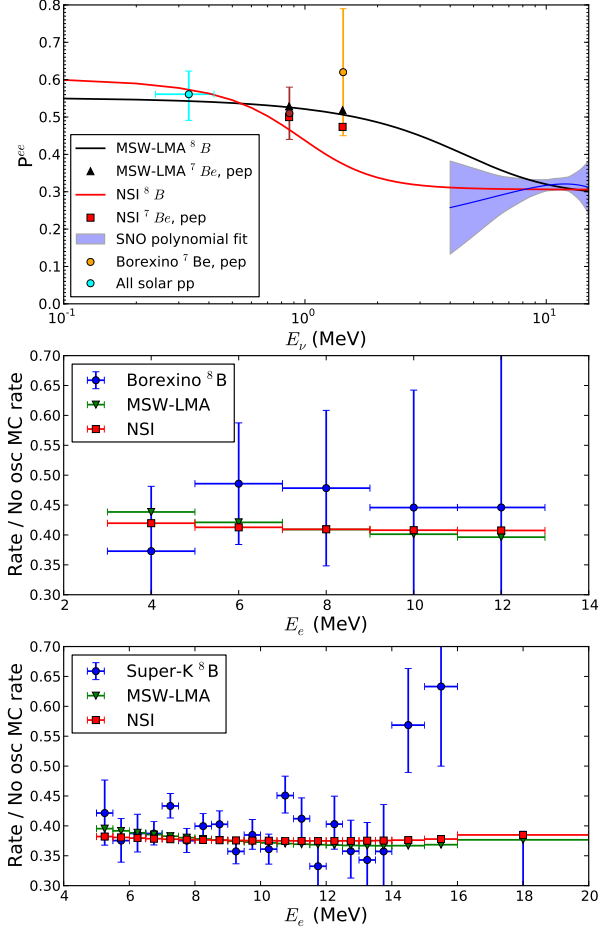


FIG. 31. (Color online) Best fit for scalar long-range force at $m_{1,0} = 0$, $\lambda = 1.56R_\odot$, $k_S = 6.73 \times 10^{-45}$, $\Delta m_{21}^2 = 7.484 \times 10^{-5} \text{eV}^2$, $\sin^2 \theta_{12} = 0.320$, $\sin^2 \theta_{13} = 0.0239$. The top plot shows the survival probability as a function of incident neutrino energy. The middle shows the best fit's predicted event rate in Borexino for each of Borexino's measured electron energy bins scaled by the GS98SF2 flux no-oscillation prediction compared to Borexino's data, and the bottom shows the same for S-K III's energy bins and data.

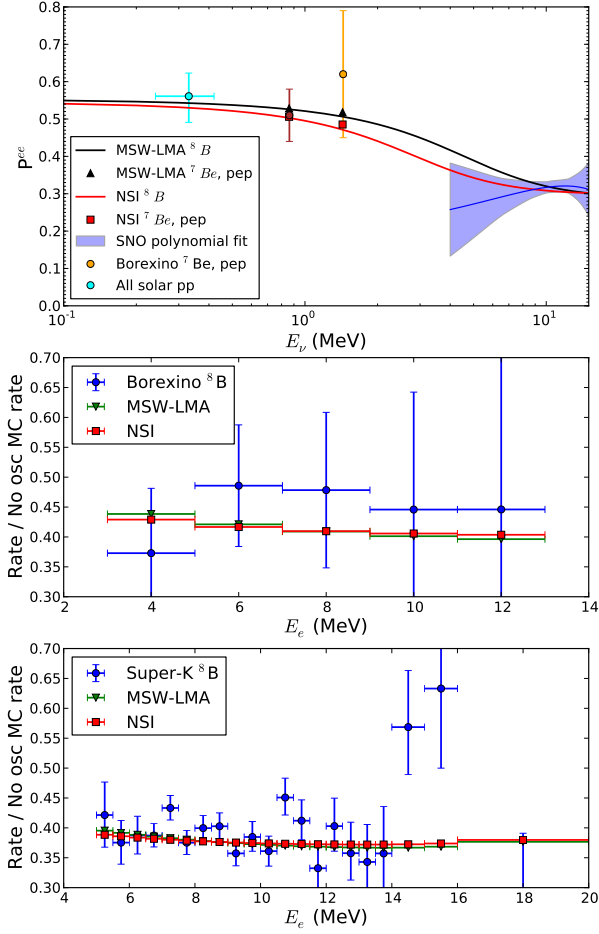


FIG. 32. (Color online) Best fit for vector long-range force at $\lambda = 16.97R_\odot$, $k_V = 3.26 \times 10^{-54}$, $\Delta m_{21}^2 = 7.487 \times 10^{-5} \text{eV}^2$, $\sin^2 \theta_{12} = 0.311$, $\sin^2 \theta_{13} = 0.0238$. The top plot shows the survival probability as a function of incident neutrino energy. The middle shows the best fit's predicted event rate in Borexino for each of Borexino's measured electron energy bins scaled by the GS98SF2 flux no-oscillation prediction compared to Borexino's data, and the bottom shows the same for S-K III's energy bins and data.